Photonic bands: simple-cubic lattice

H. Sami Sözüer*

Department of Physics and Astronomy, University of Wyoming, Laramie, Wyoming 82071

Joseph W. Haus*

Research Center for Advanced Science and Technology, University of Tokyo, 4-6-1 Komaba, Meguro-ku, Tokyo 153, Japan

Received May 18, 1992; revised manuscript received September 4, 1992

Photonic band structures have been calculated for various structures with the periodicity of the simple-cubic lattice. Band gaps have been found, and the conditions for the appearances of such gaps are discussed. The effective long-wavelength dielectric constant is calculated and compared with the predictions of effective-medium and Maxwell–Garnett theories.

1. INTRODUCTION

It was suggested by Purcell[1] that spontaneous emission by quantum systems is not a fixed property but is subject to modification when the modes of the electromagnetic field are modified. A number of interesting experimental[2–4] and theoretical[5,6] studies with metallic cavities have shown the basic soundness of the idea. However, since metallic cavities can be rather lossy, the use of periodic dielectric structures was proposed[7] as a practical means of altering the electromagnetic field modes. We observed[8] that one would obtain exactly the same photonic band structure if the dielectric permittivity $\epsilon(\mathbf{r})$ and the magnetic permeability $\mu(\mathbf{r})$ were interchanged. One could further argue that other types of periodic microstructure, such as those made from combination dielectric and paramagnetic materials or superconductors, could also lead to a strong modification of the free-space electromagnetic modes.

Interest in these materials stems from the variety of potential applications. The initial search for microstructures that were expected to possess a photonic band gap concentrated on the face-centered-cubic (fcc) lattice. Microstructures that consisted of dielectric spheres embedded in a host with a low dielectric constant and of spherical voids within a dielectric material were examined.[9] Experimental and computational[10–12] efforts focused on the second and the third bands, where a gap was expected. However, no 2–3 band gap was found in these structures because of a degeneracy at the W point of the fcc Brillouin zone (BZ). We recently demonstrated[8] the existence of a gap between the eighth and ninth bands for spherical voids in a fcc. The diamond lattice,[12,13] gridlike structures,[14] and spheroidal "atoms"[15] in the fcc lattice were explored in other attempts at finding a band gap.

Previously we made a detailed investigation[8,15] of the convergence of the plane-wave method used to solve Maxwell's equations in periodic dielectric media. We used two complementary methods and found that the convergence rate can be quite slow, depending on the type of dielectric medium. The reason for the slow convergence is the discontinuity of the dielectric function and the electromagnetic fields. A well-known pathology associated with the Fourier transform of a discontinuous function is the Gibbs phenomenon, in which the partial Fourier sums fluctuate wildly around the point of discontinuity. Many of the large Fourier components contribute, because a discontinuity can, after all, be viewed as an infinitely rapid oscillation. The problem can be partially overcome by expanding the better-behaved field (**E**, **D**, **B**, or **H**) in a Fourier series. The expansion of the more pathological field can result in gross inaccuracies. Not only can one misidentify a pseudogap as a large gap, but one can also completely miss gaps between other bands.[8] For example, for closely packed dielectric spheres in the diamond structure, the band 2–3 gap is at most ~3%, and it disappears rapidly when the sphere radius is reduced. On the other hand, for these cases there is a much larger gap between the eighth and the ninth bands, which was not reported. When the spheres overlap in the diamond lattice, we also find large gaps.

We also interpreted $\epsilon(\mathbf{r})$ as the weight function and showed that its relative fluctuation from its spatial average provides a measure of deviation from the free-photon problem. When we write $\epsilon(\mathbf{r}) = \bar{\epsilon}[1 + \epsilon_r(\mathbf{r})]$, where $\bar{\epsilon}$ is the spatial average of $\epsilon(\mathbf{r})$, it becomes clear that $\bar{\epsilon}$ is an overall scaling factor and that $\|\epsilon_r\| \equiv \|\epsilon_{\text{fluc}}\|/\bar{\epsilon}$ is the perturbation parameter. We indeed find that, when $\|\epsilon_r\| \sim 1$ or larger, then significant deviations from the free-photon problem, such as band gaps, begin to appear.

The study of photonic bands with the periodicity of the simple-cubic (sc) lattice is warranted because of the simplicity of the geometry, which translates into easier and more economical fabrication techniques that can be employed. The sc lattice also provides a framework in which structures with different topologies can be investigated, since previous computational results indicate a strong relationship between topology and the appearance of photonic band gaps. We report here the results for spheres and scaffold structures.

0740-3224/93/020296-07$05.00

2. METHOD

We start with Maxwell's equations for $\mathscr{E}$ and $\mathscr{H}$ in a dielectric medium:

$$\nabla \times \nabla \times \mathscr{E}(\mathbf{r},t) + \frac{1}{c^2}\frac{\partial^2}{\partial t^2}\epsilon(\mathbf{r})\mathscr{E}(\mathbf{r},t) = 0, \tag{1}$$

$$\nabla \times \eta(\mathbf{r})\nabla \times \mathscr{H}(\mathbf{r},t) + \frac{1}{c^2}\frac{\partial^2}{\partial t^2}\mathscr{H}(\mathbf{r},t) = 0, \tag{2}$$

where $\eta(\mathbf{r}) \equiv 1/\epsilon(\mathbf{r})$ and $\epsilon(\mathbf{r})$ is linear, locally isotropic, positive-definite, and periodic with lattice vectors $\mathbf{R}$ and

$$\epsilon(\mathbf{r}) = \epsilon(\mathbf{r} - \mathbf{R}) > 0. \tag{3}$$

The eigenfunctions of Eqs. (1) and (2) are Bloch functions of the form

$$\mathbf{E}_{n\mathbf{k}}(\mathbf{r},t) = \exp[i(\mathbf{k}\cdot\mathbf{r} - \omega_{n\mathbf{k}}t)]\sum_{\mathbf{G}}\mathbf{E}_{n\mathbf{k}}(\mathbf{G})\exp[i(\mathbf{G}\cdot\mathbf{r})], \tag{4}$$

$$\mathbf{H}_{n\mathbf{k}}(\mathbf{r},t) = \exp[i(\mathbf{k}\cdot\mathbf{r} - \omega_{n\mathbf{k}}t)]\sum_{\mathbf{G}}\mathbf{H}_{n\mathbf{k}}(\mathbf{G})\exp[i(\mathbf{G}\cdot\mathbf{r})], \tag{5}$$

where $\mathbf{G}$ is a reciprocal lattice vector and the Fourier coefficients $\mathbf{E}_{\mathbf{G}} \equiv \mathbf{E}_{n\mathbf{k}}(\mathbf{G})$ and $\mathbf{H}_{\mathbf{G}}$, respectively, satisfy the infinite-dimensional matrix equations

$$(\mathbf{k}+\mathbf{G}) \times [(\mathbf{k}+\mathbf{G}) \times \mathbf{E}_{\mathbf{G}}] + \frac{\omega^2}{c^2}\sum_{\mathbf{G}'}\epsilon_{\mathbf{G}\mathbf{G}'}\mathbf{E}_{\mathbf{G}'} = 0, \tag{6}$$

$$(\mathbf{k}+\mathbf{G}) \times \left[\sum_{\mathbf{G}'}\eta_{\mathbf{G}\mathbf{G}'}(\mathbf{k}+\mathbf{G}') \times \mathbf{H}_{\mathbf{G}'}\right] + \frac{\omega^2}{c^2}\mathbf{H}_{\mathbf{G}} = 0, \tag{7}$$

with $\epsilon_{\mathbf{G}\mathbf{G}'} \equiv \epsilon(\mathbf{G}-\mathbf{G}')$ and $\eta_{\mathbf{G}\mathbf{G}'} \equiv \eta(\mathbf{G}-\mathbf{G}')$. Equation (6) is an infinite-dimensional generalized Hermitian eigenproblem, hereafter referred to as the E method, while Eq. (7) is an ordinary Hermitian eigenproblem, which we will call the H method. The Bloch functions satisfy the following orthogonality relations[8]:

$$\int_{\text{all }\mathbf{r}} d\mathbf{r}\, \exp[-i(\mathbf{k}-\mathbf{k}')\cdot\mathbf{r}]\epsilon(\mathbf{r})\mathbf{E}_{n'\mathbf{k}'}{}^*(\mathbf{r})\cdot\mathbf{E}_{n\mathbf{k}}(\mathbf{r}) = C_{n\mathbf{k}}\delta_{nn'}\,\delta(\mathbf{k}-\mathbf{k}'), \tag{8}$$

$$\int_{\text{all }\mathbf{r}} d\mathbf{r}\, \exp[-i(\mathbf{k}-\mathbf{k}')\cdot\mathbf{r}]\mathbf{H}_{n'\mathbf{k}'}{}^*(\mathbf{r})\cdot\mathbf{H}_{n\mathbf{k}}(\mathbf{r}) = C'_{n\mathbf{k}}\delta_{nn'}\,\delta(\mathbf{k}-\mathbf{k}'), \tag{9}$$

where $C_{n\mathbf{k}}$ and $C'_{n\mathbf{k}}$ are real and positive normalization constants. It is important to note that the $\mathscr{E}$ field is normalized with $\epsilon(\mathbf{r})$ as the weight function. Although the two formulations, the E and the H methods, would yield the same spectrum when an infinite number of plane waves are included, the truncated forms yield, in general, quite different spectra even when as many as a few thousand plane waves are used.

With $\nabla\cdot\nabla\times\mathscr{E} = 0$ and $\nabla\cdot\mathscr{H} = 0$, the $3N \times 3N$ matrix equations (6) and (7) can be cast into $2N \times 2N$ ordinary Hermitian forms, which are computationally more efficient. Hence the E method is identical to the method of Ho *et al.*,[12] while the H method uses the same matrix equation with $\tilde{\epsilon}_{\mathbf{G}\mathbf{G}'}{}^{-1}$ replaced with $\eta_{\mathbf{G}\mathbf{G}'}$.

Following Zhang and Satpathy,[11] one could also start with the equation satisfied by the $\mathscr{D}$ field,

$$\nabla \times \nabla \times \eta(\mathbf{r})\mathscr{D}(\mathbf{r},t) + \frac{1}{c^2}\frac{\partial^2}{\partial t^2}\mathscr{D}(\mathbf{r},t) = 0. \tag{10}$$

This approach was shown to be equivalent to the H method.[8]

The dielectric function is written as

$$\epsilon(\mathbf{r}) = \epsilon_b + \sum_{\mathbf{R}}\epsilon_0(\mathbf{r}-\mathbf{R}), \tag{11}$$

where ϵ_b is the dielectric constant of the background and $\mathbf{R}$ is a lattice vector. Its Fourier transform (FT) is

$$\epsilon(\mathbf{G}) = \frac{1}{V_{\text{cell}}}\int_{\text{WS cell}} d\mathbf{r}\, \exp(-i\mathbf{G}\cdot\mathbf{r})\epsilon(\mathbf{r}) = \epsilon_b\delta_{\mathbf{G}0} + \frac{1}{V_{\text{cell}}}\int_{\text{all }\mathbf{r}} d\mathbf{r}\, \exp(-i\mathbf{G}\cdot\mathbf{r})\epsilon_0(\mathbf{r}), \tag{12}$$

where WS stands for Wigner–Seitz; a similar expression holds for $\eta(\mathbf{G})$.

The lowest-order Fourier expansion for each method yields the two possible extreme limits for the effective long-wavelength dielectric constant ϵ_{eff}. This property gives the methods a complementary nature, since, as the number of plane waves used in the expansion is increased, the methods approach a common limit from two extreme starting points.

3. SPHERES

For isolated spheres centered at each lattice site, the dielectric function is expressed as in Eq. (11) with

$$\epsilon_0(\mathbf{r}) = (\epsilon_a - \epsilon_b)\theta(\mathbf{R}_s - |\mathbf{r}|), \tag{13}$$

where ϵ_a is the dielectric constant inside the spheres, R_s is the radius of the spheres,[16] and $\theta(x)$ is the unit step function. Its FT is

$$\epsilon(\mathbf{G}) = \epsilon_b\delta_{\mathbf{G}0} + 3\beta(\epsilon_a - \epsilon_b)\frac{\sin x - x\cos x}{x^3}, \tag{14}$$

where β is the volume fraction of the a-type material, $x \equiv GR_s$, and $\mathbf{G}$ is a reciprocal lattice vector.

For sc structures in which dielectric spheres are placed in an air background, we find no gap when the spheres are isolated. As the spheres become larger and approach the close-packed structure, a direct transition gap between the fifth and the sixth bands opens.[17] At the close-packed ratio this may even be a small gap, but the convergence of either method is not good enough to confirm this conjecture.

With air spheres in a dielectric background we observed direct transition gaps between the second and the third bands and between the fifth and the sixth. Moreover, these direct transition gaps tend to widen as the radius of the spheres is increased. The convergence of the E method is quite good for these structures, as was the case

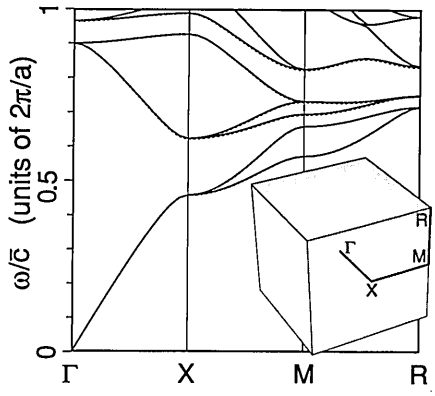

Fig. 1. Photonic band structure for close-packed air spheres in the sc lattice. $\epsilon_b = 13$, $\epsilon_a = 1$, and $\beta = \pi/6$, with 750 plane waves (solid curves) by the E method. Also plotted are the lowest six bands, calculated with only 81 plane waves (overlapping dashed curves) for comparison. $\bar{c} \equiv c/\sqrt{\bar{\epsilon}}$, where $\bar{\epsilon}$ is the spatial average of $\epsilon(\mathbf{r})$. The inset shows the path in the sc BZ.

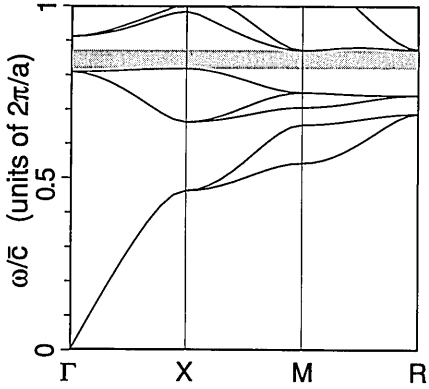

Fig. 2. Photonic band structure for overlapping air spheres in the sc lattice. $\epsilon_b = 13$, $\epsilon_a = 1$, and $\beta = 0.81$. The E method was used with 750 plane waves.

for air spheres in the fcc and the diamond structures. In Fig. 1 we plot the band structure for a dielectric contrast of 13 when the spheres are closely packed, i.e., for $\beta = \pi/6$. When the spheres overlap, the direct transition gap between the fifth and the sixth bands widens and becomes a full gap at $\beta \approx 0.66$. It is also interesting to note that $\|\epsilon_r\| \approx 1.1$ when the gap opens. The 5–6 band gap peaks to $\sim 7\%$ near $\beta \approx 0.81$. We plot the band structure for this case in Fig. 2. The gap vanishes near $\beta \approx 0.92$, where the radius of the spheres $R_s \approx 4.2$. When $R_s = \pi\sqrt{2} = 4.44$, the background medium breaks up into isolated star-shaped islands with six spikes along the Cartesian axes. Both the a- and the b-type materials are connected for $\pi \leq R_s \leq \pi\sqrt{2}$, and the structures for which there is a gap fall in this region (Fig. 3). On the other hand, the second and third bands do not separate enough to yield a complete gap when R_s is varied.

For $\beta > \pi/6$, we divided the sc unit cell into a $400 \times 400 \times 400$ grid to FT $\epsilon(\mathbf{r})$. For the case $\beta \approx 0.81$, we tested the effect of grid size on the 5–6 band gap and found it to be negligible. With an $800 \times 800 \times 800$ FT grid and 1503 plane waves, the E method yields a 5–6 band gap of 6.64%, whereas the H method yields 5.94%; the results are the same, to within 3 digits, as those obtained with the $400 \times 400 \times 400$ grid. On the other hand, the gap tended to increase with either method as N was increased, so we are quite confident of the presence of a gap for this structure.

4. SCAFFOLD STRUCTURES

The results of Section 3 warrant the investigation of a similar structure with the same topology but a simpler geometry. By this we mean a structure that is obtained from the overlapping-spheres structure by a continuous deformation without cutting or pasting. The possibilities are clearly endless, but two stand out in particular. One structure is rods of square cross section along the Cartesian axes (Fig. 4). In the simplest such structure the faces of the rods are oriented parallel to those of the unit cell. Structures with all flat faces at right angles are amenable to fabrication at a submicrometer scale by epi-

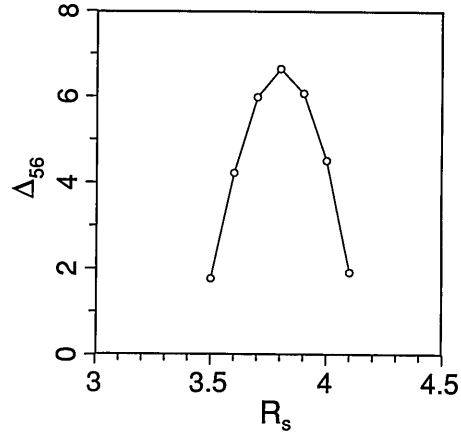

Fig. 3. Relative photonic band gap versus the radius R_s of air spheres in the sc lattice. $\epsilon_b = 13$ and $\epsilon_a = 1$. $R_s = \pi$ corresponds to the close-packed case, and at $R_s = \pi\sqrt{2}$ the background medium becomes disconnected.

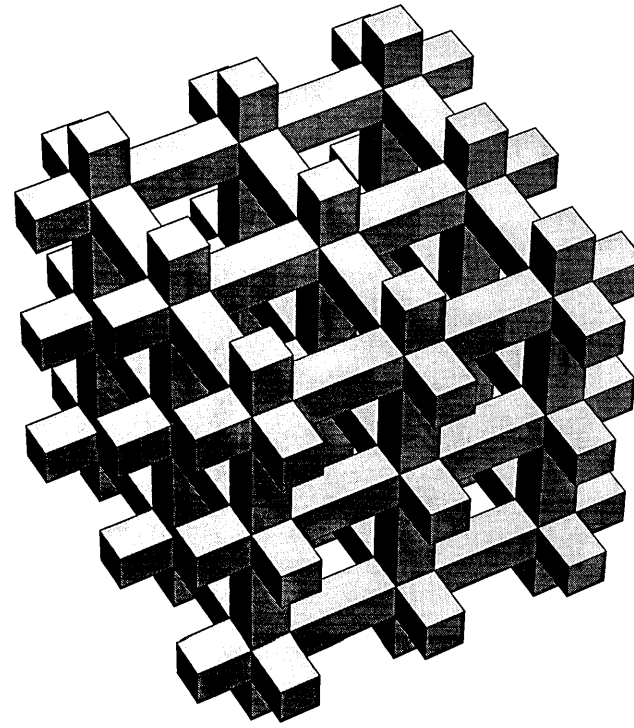

Fig. 4. Square-rod structure. A $3 \times 3 \times 3$ section is shown.

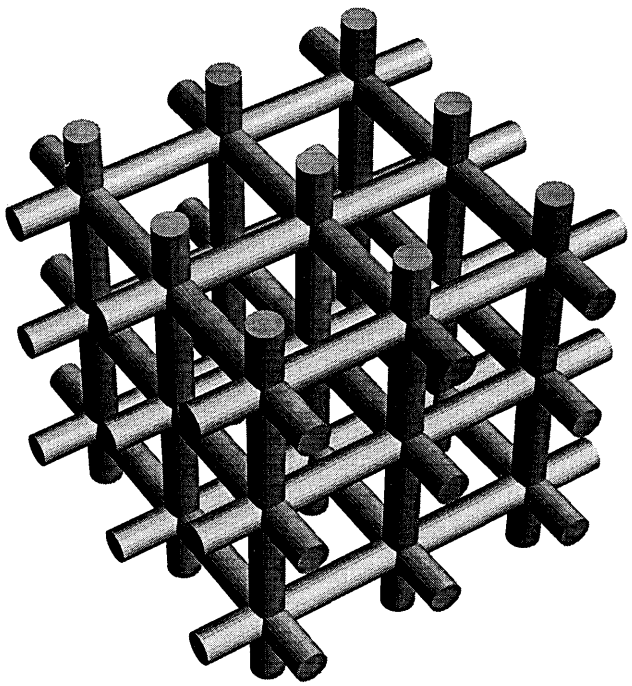

Fig. 5. Circular-rod structure. A $3 \times 3 \times 3$ section is shown.

taxial methods. The original structure proposed by Yablonovitch,[7] namely, the three-dimensional checkerboard pattern, also had flat faces at right angles but did not yield a gap, because of the aforementioned degeneracy at the W point of the fcc BZ.[18] We also investigated a similar structure with rods of circular cross section in the sc lattice (Fig. 5), which is especially well suited for ion-etching techniques.

A. Square-Rod Structures

The dielectric function for this structure is expressed as in Eq. (11), with

$$\epsilon_0(\mathbf{r}) = (\epsilon_a - \epsilon_b)\Bigg[\theta(\pi - |x|)\theta\left(\frac{s}{2} - |y|\right)\theta\left(\frac{s}{2} - |z|\right) + \theta\left(\frac{s}{2} - |x|\right)\theta(\pi - |y|)\theta\left(\frac{s}{2} - |z|\right) + \theta\left(\frac{s}{2} - |x|\right)\theta\left(\frac{s}{2} - |y|\right)\theta(\pi - |z|) - 2\theta\left(\frac{s}{2} - |x|\right)\theta\left(\frac{s}{2} - |y|\right)\theta\left(\frac{s}{2} - |z|\right)\Bigg], \quad (15)$$

where s is the length of a side of the square; the first three terms in square brackets are the contributions from each rod along the x, y, and z axes, and the last term corrects for the overcounting of the cubic region where the three rods intersect. The FT of $\epsilon(\mathbf{r})$ is then written as

$$\epsilon(\mathbf{G}) = \epsilon_b\delta_{\mathbf{G}0} + (\epsilon_a - \epsilon_b)\left(\frac{2\pi s^2}{V_{\text{cell}}}\frac{\sin Y}{Y}\frac{\sin Z}{Z}\delta_{G_x0} + \frac{2\pi s^2}{V_{\text{cell}}}\frac{\sin Z}{Z}\frac{\sin X}{X}\delta_{G_y0} + \frac{2\pi s^2}{V_{\text{cell}}}\frac{\sin X}{X}\frac{\sin Y}{Y}\delta_{G_z0} - 2\frac{s^3}{V_{\text{cell}}}\frac{\sin X}{X}\frac{\sin Y}{Y}\frac{\sin Z}{Z}\right), \quad (16)$$

where $X \equiv G_x s/2$, $Y \equiv G_y s/2$, $Z \equiv G_z s/2$, and $V_{\text{cell}} = (2\pi)^3$ is the volume of the sc unit cell.

This structure is also interesting because its topology is the same for all values of β. Furthermore, the a- and the b-type regions, except for size, have exactly the same geometry, and for $\beta = 0.5$ the two regions are identical. β again refers to the volume fraction of the a-type material.

Because of the sharp edges and corners of this structure we anticipated a convergence problem, and indeed convergence is not a trivial issue for these structures. We tried both cubic and spherical truncations in **G** space and found that spherical truncation is slightly better for the same number of plane waves. To get a feeling for the relative convergence rates of the two methods, we first plot in Fig. 6 ϵ_{eff}^E and ϵ_{eff}^H versus $N^{-1/3}$ for the case $\beta = 0.82$, for which we observed the largest gap. The convergence of the E method is clearly better than that of the H method, but it is also clear that the E method is by no means perfect, although an extrapolation in $N^{-1/3} \to 0$ does produce consistent results. Since the truncation volume in **G** space is spherical, $N \sim G_{\text{max}}{}^3$ where N is the number of plane waves retained in the Fourier expansion. Thus

$$N^{-1/3} \sim 1/G_{\text{max}}$$

is the approximate linear resolution and hence serves as a suitable extrapolation parameter. Figure 7 is a plot of ϵ_{eff} that is obtained from such an extrapolation. Also plotted are the Hashin–Shtrikman bounds[19] and the effective-medium result[20] for comparison. In contrast to the case of spheres, ϵ_{eff} is well modeled by the effective-medium theory for these types of structures. Figure 8 is the band structure for $\beta \approx 0.82$, and Fig. 9 is the density of states computed with a random sample of 300 **k** points in the BZ. The 2–3 band gap increases with N for both methods (Fig. 10), which makes us quite sure that it is reliable.

1. *Scaffold Structures in the Face-Centered-Cubic Lattice*

If one were to drill cylindrical holes of square cross section along the x, y, and z directions through each lattice site in the fcc lattice, one would end up with the same structure as above. This is because the sc lattice is also a fcc lattice with a basis, with lattice constant $a_{\text{fcc}} = 2a_{\text{sc}}$ and basis vectors $\mathbf{b}_{1,2} = \pm(0,0,1)a_{\text{fcc}}/4$. The reciprocal vectors of

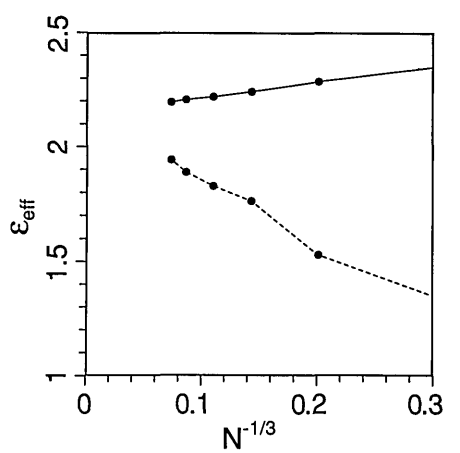

Fig. 6. $\epsilon_{\text{eff}}^{\text{E}}$ (solid) and $\epsilon_{\text{eff}}^{\text{H}}$ (dashed) for the square-rod structure as a function of $N^{-1/3}$. $\epsilon_b = 13$, $\epsilon_a = 1$, and $\beta = 0.82$.

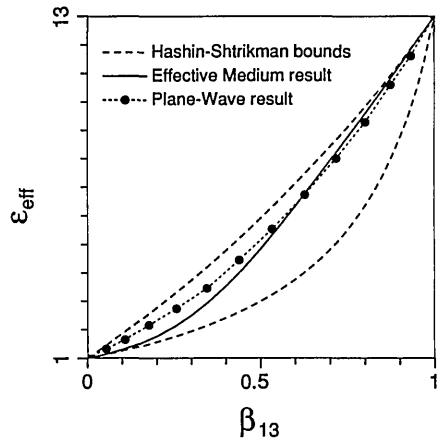

Fig. 7. ϵ_{eff} calculated with the plane-wave method (●) for the square-rod structure in the sc lattice. Also plotted are the Hashin–Shtrikman bounds (Maxwell–Garnett results) (long dashed curves) and the effective-medium result (solid curve). β_{13} is the volume fraction of the $\epsilon = 13$ material.

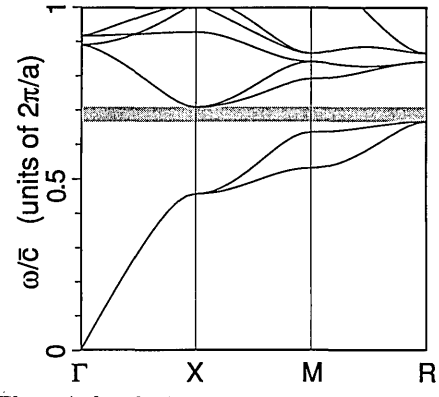

Fig. 8. Photonic bands for the square-rod structure in the sc lattice. $\epsilon_b = 13$, $\epsilon_a = 1$, and $\beta = 0.82$.

the fcc lattice are expressed as

$$\mathbf{G}_{\text{fcc}} = (n_x, n_y, n_z)\frac{2\pi}{a_{\text{fcc}}}, \qquad n_x, n_y, n_z \text{ all even or all odd}, \tag{17}$$

whereas the reciprocal vectors of the sc lattice are

$$\mathbf{G}_{\text{sc}} = (m_x, m_y, m_z)\frac{2\pi}{a_{\text{sc}}}, \qquad m_x, m_y, m_z \text{ any integers}. \tag{18}$$

Noting that $a_{\text{fcc}} = 2a_{\text{sc}}$, one obtains

$$\mathbf{G}_{\text{sc}} = (m_x, m_y, m_z)\frac{2\pi}{a_{\text{fcc}}}2, \qquad m_x, m_y, m_z \text{ any integers}, \tag{19}$$

$$\mathbf{G}_{\text{sc}} = (m_x', m_y', m_z')\frac{2\pi}{a_{\text{fcc}}}, \qquad m_x', m_y', m_z' \text{ even integers}. \tag{20}$$

Thus the fcc reciprocal lattice has twice as many points. Eliminating the odd points, one obtains the sc reciprocal lattice. Hence $\epsilon(\mathbf{G}_{\text{fcc}}) = 0$ for odd $\mathbf{G}_{\text{fcc}}$ and $\epsilon(\mathbf{G}_{\text{fcc}}) = \epsilon(\mathbf{G}_{\text{sc}})$ for even $\mathbf{G}_{\text{fcc}}$. An immediate consequence of this property is that the Bloch functions in the fcc lattice separate into odd and even types, since there is no mixing between the two types of Bloch functions that arise from the matrix elements $\epsilon(\mathbf{G} - \mathbf{G}')$ with $\mathbf{G} - \mathbf{G}'$ odd. Hence

$$\mathbf{E}_{n\mathbf{k}}^{\text{even}}(\mathbf{r}, t) = \exp[i(\mathbf{k}\cdot\mathbf{r} - \omega_{n\mathbf{k}}t)] \sum_{\text{even } \mathbf{G}} \mathbf{E}_{n\mathbf{k}}(\mathbf{G})\exp[i(\mathbf{G}\cdot\mathbf{r})], \tag{21}$$

$$\mathbf{E}_{n\mathbf{k}}^{\text{odd}}(\mathbf{r}, t) = \exp[i(\mathbf{k}\cdot\mathbf{r} - \omega_{n\mathbf{k}}t)] \sum_{\text{odd } \mathbf{G}} \mathbf{E}_{n\mathbf{k}}(\mathbf{G})\exp[i(\mathbf{G}\cdot\mathbf{r})]. \tag{22}$$

This separation is used further to reduce the dimensionality by a factor of 2. Hence the problem in the fcc lattice is solved in two steps; one first expands the fields in the odd reciprocal basis, then expands the fields in the even basis, and then combines the odd and even bands. This technique indeed yields the same band structure as that obtained when the complete fcc reciprocal basis is used. Overall, however, treating the problem in the sc lattice is more economical by a factor of approximately 2.

The band structure calculated with the E method for 750 plane waves is plotted in Fig. 11. It is worth noting a number of interesting features for comparison. In the sc BZ $X_{\text{sc}} = (0.5, 0, 0)2\pi/a_{\text{sc}}$, and in the fcc BZ $X_{\text{fcc}} = (1, 0, 0)2\pi/a_{\text{fcc}}$. Noting that $a_{\text{fcc}} = 2a_{\text{sc}}$, we find that $X_{\text{fcc}} = X_{\text{sc}}$. On the other hand, $R_{\text{sc}} = (0.5, 0.5, 0.5)2\pi/a_{\text{sc}} =$

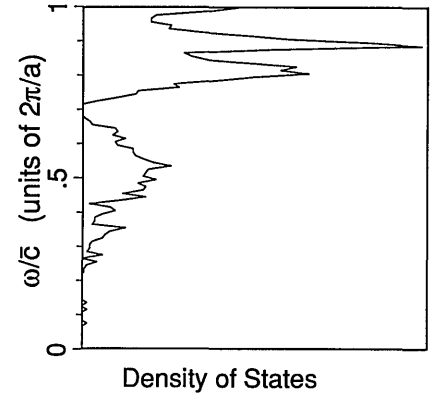

Fig. 9. Density of states computed from a random sample of 300 **k** points in the BZ for the same dielectric structure as in Fig. 8.

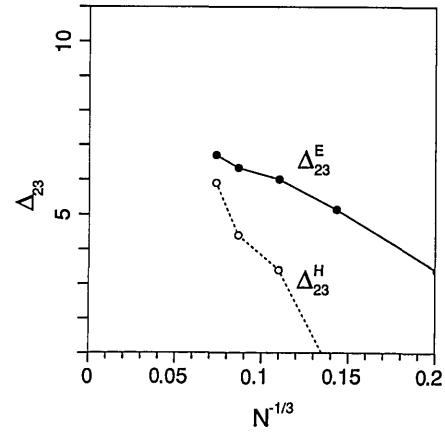

Fig. 10. Photonic band gap versus $N^{-1/3}$ for the same structure as in Fig. 8 with the E and the H methods.

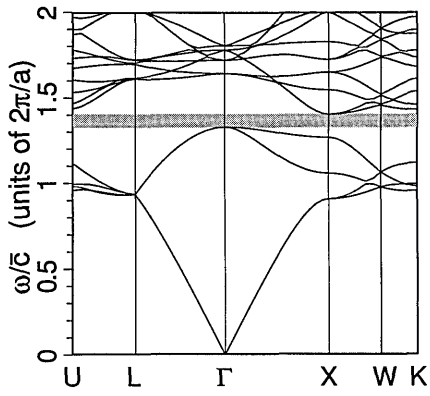

Fig. 11. Photonic bands for the same dielectric structure as in Fig. 8, calculated within the periodicity of the fcc lattice. The vertical scale is different from that of Fig. 8 because $a_{\mathrm{fcc}} = 2a_{\mathrm{sc}}$.

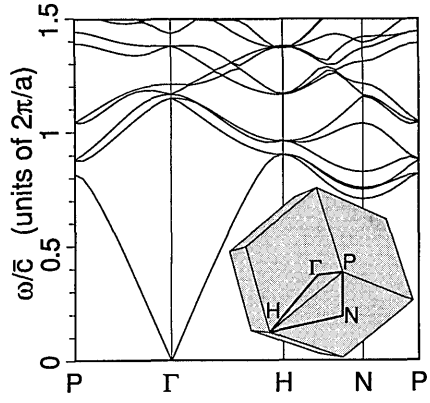

Fig. 12. Photonic bands for the scaffold structure in the bcc lattice. $\epsilon_b = 13$, $\epsilon_a = 1$, and $\beta = 0.84$. 1481 plane waves were used with the E method. The H method yields the same degeneracies, but its convergence is slow.

$(1,1,1)2\pi/a_{\mathrm{fcc}}$. But the point $(1,1,1)2\pi/a_{\mathrm{fcc}}$ is outside the fcc BZ, and since it is an fcc reciprocal lattice vector, it is equivalent to Γ_{fcc}. Hence R_{sc} is equivalent to Γ_{fcc} for this problem. This equivalence is also apparent from Figs. 8 and 12, in which the lower value of the bandgap occurs at $R_{\mathrm{sc}} \sim \Gamma_{\mathrm{fcc}}$ and the higher value at $X_{\mathrm{fcc}} = X_{\mathrm{sc}}$. The reason that the band gap is between the fourth and the fifth bands in Fig. 11 is that the fcc BZ is smaller than the sc BZ.

2. Scaffold Structures in the Body-Centered-Cubic Lattice

At this point one is led to investigate the dielectric structure obtained by the same prescription in the remaining Bravais lattice with cubic symmetry, the body-centered-cubic (bcc) lattice. These are structures obtained by drilling cylindrical holes of square cross section along the x, y, and z directions through each bcc lattice site; $\epsilon(\mathbf{r})$ can be written in the form of Eqs. (11) and (15), where, of course, $\mathbf{R}$ is now a bcc lattice vector. This structure is quite different, because one now has two scaffolds, interlaced but disjoint, with one scaffold displaced by $(1,1,1)a/2$ relative to the other. The two scaffolds, of course, have the same dielectric constant ϵ_a. We calculated the band structure for this case for $\beta = 0.84$ and failed to find any gaps (Fig. 12).

B. Circular-Rod Structures

The dielectric function for this structure is expressed as in Eq. (11), with

$$\begin{aligned}\epsilon_0(\mathbf{r}) = (\epsilon_a - \epsilon_b)[&\theta(\pi - |x|)\theta(R_c - \rho_{yz}) \\ &- \theta(R_c - |x|)\theta(R_c - \rho_{yz}) \\ &+ \theta(\pi - |y|)\theta(R_c - \rho_{zx}) - \theta(R_c - |y|)\theta(R_c - \rho_{zx}) \\ &+ \theta(\pi - |z|)\theta(R_c - \rho_{xy}) - \theta(R_c - |z|)\theta(R_c - \rho_{xy}) \\ &+ \theta(R_c - |x|)\theta(R_c - |y|)\theta(R_c - |z|)] - C_0(\mathbf{r}),\end{aligned} \tag{23}$$

where $\epsilon(\mathbf{r}) = \epsilon_a$ inside the cylinders, R_c is the radius of the cylinders, and $\rho_{xy} \equiv (x^2 + y^2)^{1/2}$, $\rho_{yz} \equiv (y^2 + z^2)^{1/2}$, and $\rho_{zx} \equiv (z^2 + x^2)^{1/2}$. The first three pairs of terms are the contributions from each rod along the x, y, and z axes minus the rod within the cube of side $2R_c$. The fourth term is the cube, and the last term is the correction for the region that is in the cube but outside of all three cylinders,

$$C_0(\mathbf{r}) = \begin{cases} \epsilon_a - \epsilon_b & \text{if } |x|, |y|, |z| < R_c, \rho_{xy}, \rho_{yz}, \rho_{zx} > R_c \\ 0 & \text{otherwise} \end{cases}. \tag{24}$$

All the terms in Eq. (23) are Fourier transformed analytically except $C_0(\mathbf{r})$, which we FT numerically by dividing the intersection cube on a $200 \times 200 \times 200$ grid. The FT of $\epsilon(\mathbf{r})$ is then written as

$$\begin{aligned}\epsilon(\mathbf{G}) = \epsilon_b \delta_{\mathbf{G}0} + (\epsilon_a - \epsilon_b)\Bigg[&\left(\frac{2\pi^2 R_c^2}{V_{\mathrm{cell}}}\right)\frac{2J_1(G_{yz}R_c)}{G_{yz}R_c}\delta_{G_x 0} \\ &- \left(\frac{2\pi R_c^3}{V_{\mathrm{cell}}}\right)\frac{\sin(G_x R_c)}{G_x R_c}\frac{2J_1(G_{yz}R_c)}{G_{yz}R_c} \\ &+ \left(\frac{2\pi^2 R_c^2}{V_{\mathrm{cell}}}\right)\frac{2J_1(G_{zx}R_c)}{G_{zx}R_c}\delta_{G_y 0} \\ &- \left(\frac{2\pi R_c^3}{V_{\mathrm{cell}}}\right)\frac{\sin(G_y R_c)}{G_y R_c}\frac{2J_1(G_{zx}R_c)}{G_{zx}R_c} \\ &+ \left(\frac{2\pi^2 R_c^2}{V_{\mathrm{cell}}}\right)\frac{2J_1(G_{xy}R_c)}{G_{xy}R_c}\delta_{G_z 0} \\ &- \left(\frac{2\pi R_c^3}{V_{\mathrm{cell}}}\right)\frac{\sin(G_z R_c)}{G_z R_c}\frac{2J_1(G_{xy}R_c)}{G_{xy}R_c} \\ &+ \left(\frac{R_c^3}{V_{\mathrm{cell}}}\right)\frac{\sin(G_x R_c)}{G_x R_c}\frac{\sin(G_y R_c)}{G_y R_c}\frac{\sin(G_z R_c)}{G_z R_c}\Bigg] \\ &- C_0(\mathbf{G}),\end{aligned} \tag{25}$$

where $J_1(x)$ is the first-order Bessel function, $G_{xy} \equiv (G_x^2 + G_y^2)^{1/2}$, $G_{yz} \equiv (G_y^2 + G_z^2)^{1/2}$, $G_{zx} \equiv (G_z^2 + G_x^2)^{1/2}$, and

$$\begin{aligned}C_0(\mathbf{G}) &= \frac{1}{V_{\mathrm{cell}}}\int \mathrm{d}\mathbf{r} C_0(\mathbf{r})\cos(\mathbf{G}\cdot\mathbf{r}) \\ &\approx \frac{1}{V_{\mathrm{cell}}}\left(\frac{R_c}{N_{\mathrm{grid}}}\right)^3 \sum_{i,j,k=-N_{\mathrm{grid}}}^{N_{\mathrm{grid}}-1} C_0(x_i, y_j, z_k) \\ &\quad \times \cos(G_x x_i + G_y y_j + G_z z_k),\end{aligned} \tag{26}$$

where $x_i \equiv (i + 0.5)R_c/N_{\mathrm{grid}}$, $y_j \equiv (j + 0.5)R_c/N_{\mathrm{grid}}$, and $z_k \equiv (k + 0.5)R_c/N_{\mathrm{grid}}$.

In Figs. 13 and 14 we plot the band structure for dielectric cylinders in an air background and air cylinders in a dielectric background, respectively. For both types of structure the air volume fraction is ~81% at the gap peak. The dielectric cylinders have a 2–3 band gap, while the air cylinders have a 5–6 band gap. As the radius of the rods varies, the direct transition gaps between the second and

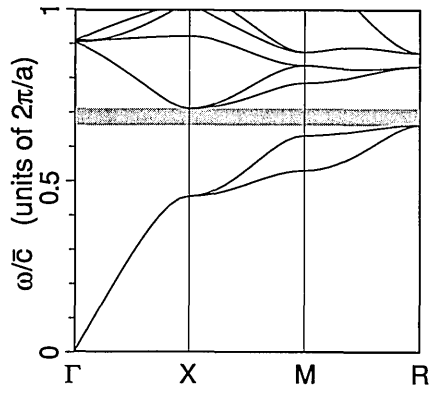

Fig. 13. Photonic band structure for the circular-dielectric-rod structure in the sc lattice. $\epsilon_b = 1$, $\epsilon_a = 13$, and $\beta = 0.19$. The radius of the dielectric rods is $R_c = 1$.

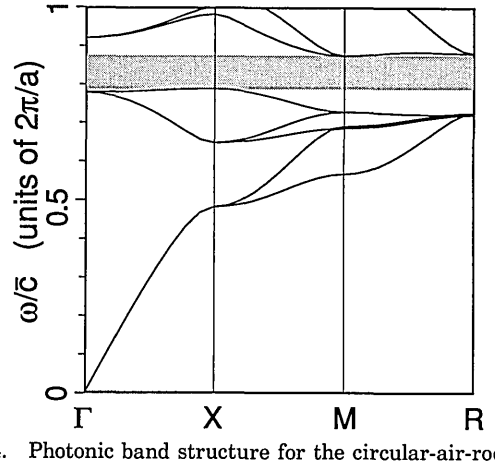

Fig. 14. Photonic band structure for the circular-air-rod structure in the sc lattice. $\epsilon_b = 13$, $\epsilon_a = 1$, and $\beta = 0.81$. The radius of the air rods is $R_c = 2.6$.

the third and between the fifth and the sixth bands vary. These figures show the results obtained with the E method, but the H method yields results that are in qualitative agreement with those plotted. Also worth noting is that the size of the gaps tends to increase with N, as in the case of square-rod structures.

5. CONCLUSION

It was proposed earlier[7,21] that the fcc lattice would be ideal for photonic band-gap formation because its Brillouin zone (BZ) is most nearly a sphere. Although this reasoning has some aesthetic appeal, the calculations so far suggest that the roundness of the BZ is not relevant and hence that the fcc lattice is not special. For example, the bcc BZ is much rounder than its sc counterpart, but we have found very small (~3%) gaps for dielectric structures with the periodicity of the bcc lattice. While there is no simple explanation as to exactly under which conditions photonic band gaps appear, our findings, coupled with those of various other studies,[12,14] suggest that the emergence of gaps seems to be related to the strength of the dielectric modulation and the connectedness of the a- and the b-type materials.[8,15]

We have shown that ϵ_{eff} for the scaffold structures is reasonably well modeled by the effective-medium theory. This is in contrast to the case of structures with the host–guest topology, where Maxwell–Garnett theory performs quite adequately.[8,22]

The use of complementary methods was an important tool in verifying our conclusions. Despite the convergence issue, one can arrive at reasonably reliable conclusions provided that the results are viewed as a sequence as one approaches the ideal limit $N \to \infty$. For many cases of interest, however, even this extrapolation scheme fails to yield consistent results. Furthermore, a realistic estimate of the Q factor for lossy materials requires the development of new methods. Candidates for future investigations could be real-space methods.[22]

ACKNOWLEDGMENTS

We acknowledge fruitful discussions with Charles M. Bowden and John P. Dowling. This research was supported by National Science Foundation grant ECS-8813028, and J. W. Haus was supported by the Defense Advanced Research Project Agency funded Optoelectronics Technology Center. The computations were performed on the IBM 3090-200S Vector Facility at the Voorhees Computing Center at Rensselaer Polytechnic Institute and on the IBM 3090-600J at the Cornell National Supercomputing Facility.

*Present address, Department of Physics, Rensselaer Polytechnic Institute, Troy, New York 12180.

REFERENCES AND NOTES

1. E. M. Purcell, Phys. Rev. **69,** 681 (1946).
2. D. Kleppner, Phys. Rev. Lett. **47,** 233 (1981).
3. R. G. Hulet, E. S. Hilfer, and D. Kleppner, Phys. Rev. Lett. **20,** 2137 (1985).
4. S. Haroche and D. Kleppner, Phys. Today **42,** 24 (1989).
5. P. W. Milonni and P. L. Knight, Opt. Commun. **9,** 119 (1973).
6. P. Meystre, in *Nonlinear Optics in Solids*, Vol. 9 of Springer Series in Wave Phenomena, O. Keller, ed. (Springer-Verlag, Berlin, 1990).
7. E. Yablonovitch, Phys. Rev. Lett. **58,** 2059 (1987).
8. H. S. Sözüer, J. W. Haus, and R. Inguva, Phys. Rev. B **45,** 13,962 (1992).
9. E. Yablonovitch and T. J. Gmitter, Phys. Rev. Lett. **63,** 1950 (1989).
10. K. M. Leung and Y. F. Liu, Phys. Rev. Lett. **65,** 2646 (1990).
11. Z. Zhang and S. Satpathy, Phys. Rev. Lett. **65,** 2650 (1990).
12. K. M. Ho, C. T. Chan, and C. M. Soukoulis, Phys. Rev. Lett. **65,** 3152 (1990).
13. C. T. Chan, K. M. Ho, and C. M. Soukoulis, Europhys. Lett. **16**(6), 563 (1991).
14. E. Yablonovitch and K. M. Leung, Physica B **175,** 81 (1991).
15. J. W. Haus, H. S. Sözüer, and R. Inguva, J. Mod. Opt. **39,** 1991 (1992).
16. Unless otherwise made clear, all lengths are in units of $a/2\pi$ and all wave vectors $(\mathbf{k},\mathbf{G})$ are in units of $2\pi/a$, where a is the length of the side of the conventional unit cell.
17. We say that there is a direct transition gap between the nth and $(n+1)$th levels when $\omega_{n+1}(\mathbf{k}) > \omega_n(\mathbf{k})$ for all $\mathbf{k}$, whereas a gap is said to exist when $\omega_{n+1}(\mathbf{k}) > \omega_n(\mathbf{k}')$ for all $\mathbf{k}$, $\mathbf{k}'$. A pseudogap, on the other hand, is a depression in the photon density of states $\rho(\omega)$.
18. H. S. Sözüer, "Photonic bands," Ph.D. dissertation (University of Wyoming, Laramie, Wyo., 1992).
19. Z. Hashin and S. Shtrikman, J. Appl. Phys. **33,** 3125 (1962).
20. W. Lamb, D. M. Wood, and N. W. Ashcroft, Phys. Rev. B **21,** 2248 (1980).
21. S. John, Phys. Rev. Lett. **58,** 2486 (1987).
22. T. Nakayama, M. Takano, K. Yakubo, and T. Yamanaka, Opt. Lett. **17,** 326 (1992); J. B. Pendry and A. MacKinnon, Phys. Rev. Lett. **69,** 2772 (1992).